Oxetane Monomers Based On the Powerful Explosive LLM-116: Improved Performance, Insensitivity, and Thermostability

Max Born[+], Konstantin Karaghiosoff, Thomas M. Klapötke,* and Michael Voggenreiter[+][a]

3-Bromomethyl-3-hydroxymethyloxetane represents an inexpensive and versatile precursor for the synthesis of 3,3-disubstituted oxetane derivatives. In the present work, its synthesis was improved and energetic oxetanes based on the explosive LLM-116 (4-amino-3,5-dinitro-1*H*-pyrazole) prepared. Reaching detonation velocities and pressures of up to 7335 ms⁻¹ and 20.9 GPa in combination with a high thermostability and insensitivity, these surpass the prior art by far. Next to a symmetric LLM-116 derivative, three asymmetric compounds were prepared using azido-, nitrato- and tetrazolyl-

moieties. All compounds were intensively characterized by vibrational-, mass- and multinuclear (^{1}H, ^{13}C, ^{14}N) NMR spectroscopy, differential scanning calorimetry and elemental analysis. The molecular structures were elucidated by single crystal X-ray diffraction. Hirshfeld analysis allowed to estimate their sensitivity next to a practical evaluation using BAM standard procedures. Their performance was calculated using the EXPLO5 V6.04 code and a small-scale shock reactivity test and initiation test demonstrated their insensitivity and performance.

Introduction

The state of the art in the field of energetic polymers is mainly represented by well-known polyethers such as GAP (glycidyl azide polymer), poly(3,3-bis(azidomethyl)oxetane) (polyBAMO), poly(3-azidomethyl-3-methyloxetane) (polyAMMO), poly(3-nitratomethyl-3-methyloxetane) (polyNIMMO) and poly(glycidyl nitrate) (polyGLYN).[1] Unfortunately, the respective monomers show performances way inferior to TNT or more recent developments in the field of secondary explosives. They can be subdivided into two groups – azides, which feature relatively high thermostability at the price of poor oxygen balance and organic nitrates with improved oxygen balance at the cost of thermostability below modern requirements.[2] Their polymers are preferred over non-energetic binders, but their energetic contribution in formulations is low. Therefore, new monomers combining higher performance and thermostability with less sensitivity are highly desirable. For example, binders prepared thereof could find application in especially safe low-vulnerability ammunitions (LOVA) and propellants.[3] In this context, a patent describes 3-bromomethyl-3-hydroxymethyloxetane (BMHMO) as very suitable starting material for the preparation
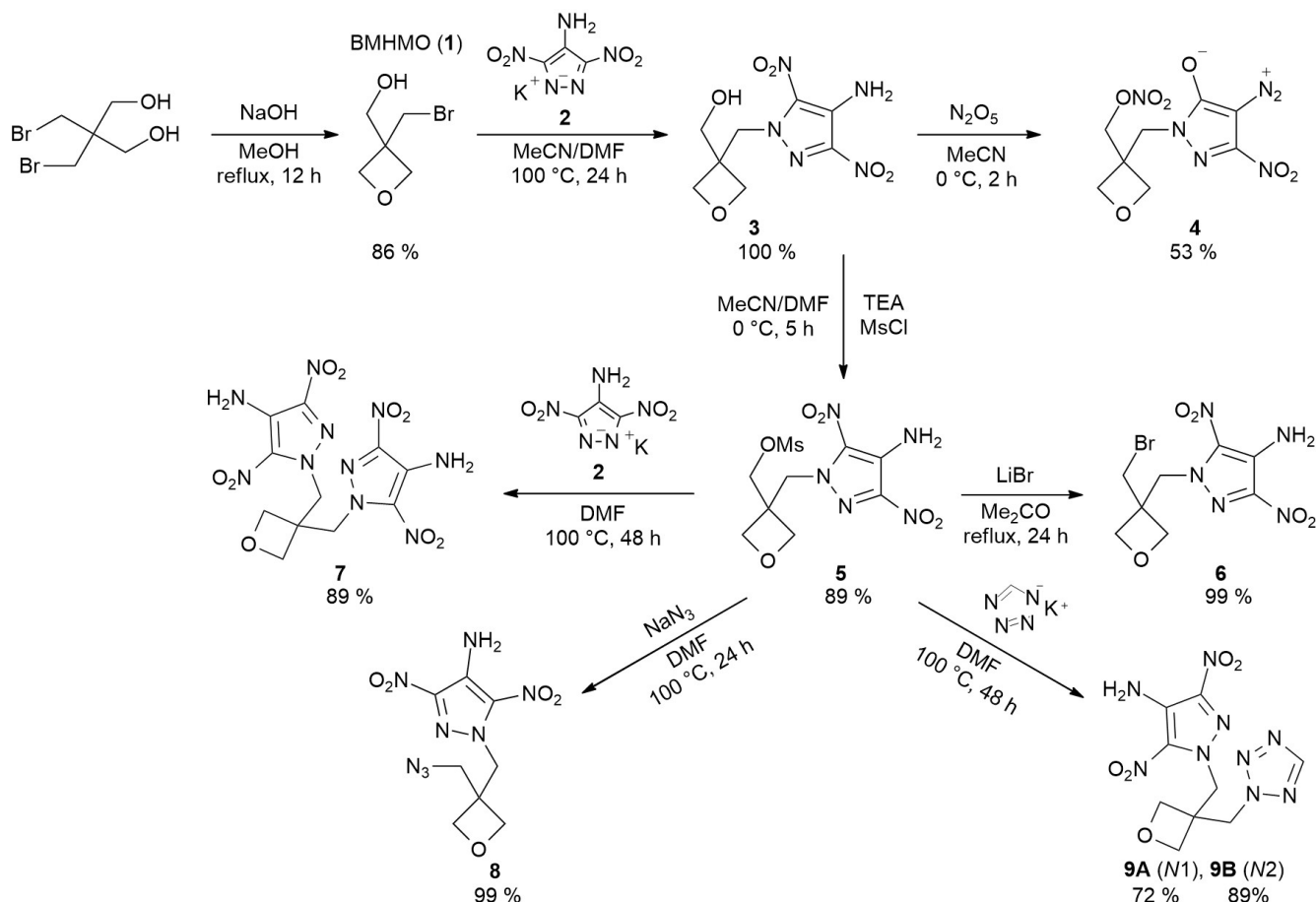
of asymmetric oxetane monomers. For instance, the preparation of the powerful compound 3-azidomethyl-3-nitratomethyloxetane is disclosed.[4] Indeed, BMHMO shows advantageous properties. It can be prepared inexpensively by Williamson ether synthesis and is chemically very versatile. For example, the excellent leaving group enables functionalization with nucleophiles and follow-up reactions with electrophiles making use of the hydroxy group may afford asymmetric species. Conversion of this group into a leaving group enables access to either symmetric or asymmetric derivatives by further substitution reactions. Beyond, the present methylene spacers diminish the adverse effect of mostly electron-withdrawing explosophoric groups on the oxetane oxygen atom. This is of advantage as the success of a cationic ring-opening polymerization strongly depends on the basicity of the oxygen atom.[5] However, the scaffold of BMHMO imposes a detrimental carbon-hydrogen ballast rendering it beneficial to use larger energetic motifs as substituents to mitigate or compensate this particular influence. For this purpose, powerful secondary explosives with functional groups like 4-amino-3,5-dinitro-1*H*-pyrazole (LLM-116 or ADNP) are very promising. ADNP was first described as protected compound in 1993 by Vinogradov and later as unprotected compound by Shevelev in 1998.[6] Since then, it has been made accessible by several synthetic routes, whereas 4-chloro-1*H*-pyrazole provides the highest yield when used as starting material.[7] ADNP impresses with a high density (1.90 g cm⁻³) and a correspondingly high detonation velocity and pressure (8680 ms⁻¹, 32.8 kbar).[8] Already in 2014, it was employed in a pilot scale study by Ek and Latypov and prepared in 200 g batches.[7] Due to its favorable properties, ADNP has been increasingly used for the synthesis of new energetic materials since 2011.[9–11] Herein, we report an significantly improved synthesis of BMHMO, rendering it an even more attractive starting material for the synthesis of energetic oxetane

[a] M. Born,[+] Prof. Dr. K. Karaghiosoff, Prof. Dr. T. M. Klapötke, M. Voggenreiter[+]
     Department of Chemistry
     Ludwig-Maximilians University of Munich
     Butenandtstr. 5–13, 81377 Munich (Germany)
     E-mail: tmk@cup.uni-muenchen.de
     Homepage: www.hedm.cup.uni-muenchen.de

[+] These authors contributed equally to this work.

ChemPlusChem

Research Article
doi.org/10.1002/cplu.202200049

Chemistry Europe
European Chemical
Societies Publishing

Scheme 1. Synthetic pathway starting with the ring-closure of 2,2-bis(bromomethyl)propane-1,3-diol toward BMHMO (**1**). Subsequent substitution using the potassium salt of LLM-116 affords compound **3**. Nitration results in target compound **4** while mesylation gives compound **5** providing access to target compounds **6**–**9** in high overall yield.
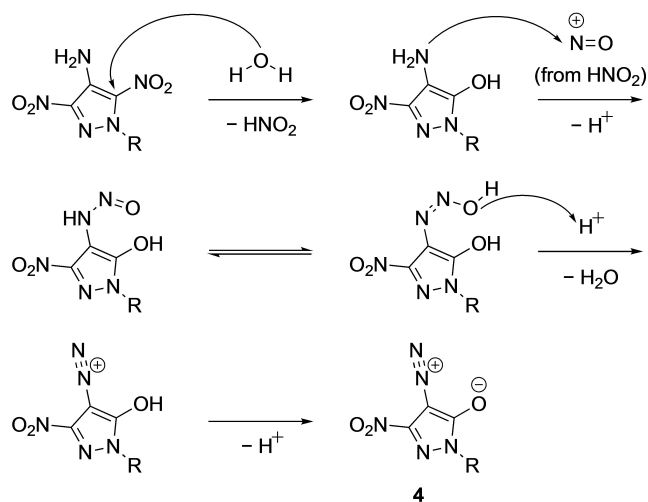
monomers. Ultimately, it was used to prepare symmetric and asymmetric derivatives based on LLM-116. Here, high yields and the preferential use of commercially available materials contribute to low costs. The molecular structures of all products were elucidated by X-ray diffraction also allowing Hirshfeld analysis which made the high insensitivity of some target compounds and the results of the SSRT and initiation test comprehensible. In terms of performance and thermostability, the target compounds are largely superior to prior art energetic oxetane monomers. Based on the fine balance of these new monomers between performance, thermostability and insensitivity, they are promising candidates for the preparation of energetic polymers with improved properties in these key-aspects.

Results and Discussion

Synthetic Procedures

The Williamson reaction to give 3-bromomethyl-3-hydroxymethyloxetane (BMHMO, **1**) was significantly improved by changing base and solvent from NaOEt/EtOH to NaOH/MeOH to give a crude yield of 93%. Subsequent vacuum distillation removed by-products (e.g., spiro-compound) and unreacted starting material to afford pure BMHMO as colorless oil in 85% (+33%) yield while the literature reports only 52% after purification.[4] Reaction of **1** with the potassium salt of 4-amino-3,5-dinitro-1H-pyrazole (K-ADNP, **2**) in DMF led to alcohol **3** which was isolated by the precipitation of inorganic salts using ethyl acetate, filtration through a Celite plug and rotary evaporation to remove all volatiles. Residual traces of DMF were co-evaporated (cold ether) to afford **3** as bright-yellow solid in quantitative yield (Scheme 1). It was tried to obtain the corresponding nitrate **4** using acetyl nitrate as mild and cost-efficient nitrating agent but several attempts failed (recovery of starting material). However, aprotic nitration using dinitrogen pentoxide was successful while minimizing the risk of undesired ring-opening of the oxetane ring by hydrolysis. Unfortunately, the pyrazole motif suffered from severe chemical changes and the zwitterionic diazonium olate **4** was obtained. Similar zwitterionic pyrazole compounds are known to literature but usually obtained by targeted diazotation reactions.[12] Fischer reported a very similar diazonium olate by nitrating the structurally related bis(4-amino-3,5-dinitropyrazolyl)methane with mixed acid followed by quenching on water.[10] However, no mechanism for the formation of this particular structure was

ChemPlusChem

Research Article
doi.org/10.1002/cplu.202200049

Chemistry
Europe
European Chemical
Societies Publishing

Scheme 2. Proposed mechanism for the formation of diazonium olate **4**.

proposed. As nitro groups are prone to act as leaving groups in aromatic nucleophilic substitution reactions, we assume a nucleophilic attack of water upon quenching. This leads to the formation of nitrous acid as source of nitrosyl cations. These cause a quick, subsequent diazotation reaction toward compound **4** (Scheme 2). Despite various solvent/anti-solvent precipitation attempts, the crude compound remained an extremely viscous oil. Ultimately, column chromatography (SiO₂, EtOAc) afforded **4** in 53% yield as orange solid. To enable further substitution reactions, compound **3** was mesylated to provide a good leaving group. Due to the tailored solvent system, methanesulfonic ester **5** precipitated as lemon-yellow solid after a short reaction time and was obtained by suction filtration in high purity and yield (85%). Since particularly weak or sterically demanding nucleophiles are not always able to readily substitute the mesyl group, compound **5** was converted to the bromo-species **6** in a Finkelstein-type reaction using lithium bromide in acetone to provide an alternative leaving group. Filtration through silica (EtOAc) to separate inorganic salts gave compound **6** in high purity and quantitative yield (Scheme 1). However, all follow-up substitution reactions were successfully performed using mesylate **5** thus avoiding this additional step. DMF was employed as solvent as it allows high reaction temperatures and removal by rotary evaporation while it dissolves sodium azide, K-ADNP and potassium tetrazol-1-ide rather well. The reaction of **5** with K-ANDP (**2**) was complete after 48 h according to TLC. The high reaction time can be explained by the steric demand of the nucleophile. All inorganic salts were separated as previously described and DMF was evaporated. The crude material was suspended in diethyl ether and collected by suction filtration to give **7** in high yield and purity (89%) as yellow solid. Compound **8** was prepared analogously from **5** using sodium azide. The same work-up routine was applied and traces of DMF removed by co-evaporation to give **8** in 99% yield. Dissolution of **8** in a small amount of acetone followed by precipitation (n-hexane) gave pure **8** as bright yellow solid without yield loss. As in case of

compound **7**, the reaction of **5** with potassium tetrazol-1-ide required a prolonged reaction time of 48 h according to TLC. The work-up was performed as described before and the crude isomeric mixture (**9A**, **9B**) was suspended in a small amount of acetone prior to the addition of an excess of diethyl ether. After suction filtration, a yield of 98% was obtained and ¹H NMR spectroscopy revealed a N1/N2 ratio of 1:2. The regioisomers were separated by refluxing the mixture in toluene and filtration of the hot suspension. The filtrate was evaporated to give pure N2-isomer (**9B**) with a yield of 89%. The filter residue contained 10% N2-isomer (¹H NMR) and was recrystallized from acetone to give 72% of N1-isomer (**9A**) also as yellow solid. Thereby, an overall yield of 84% (N1, N2) was achieved without column chromatography.

Crystallography

Single crystals of the following compounds were obtained by slow evaporation of their solutions using ethyl acetate (**4**, **8**), DMF (**7**), toluene (**9B**) and acetone (**9A**). Detailed crystallographic data can be found in the Supporting Information. Compound **4** crystallizes in the monoclinic space group P2₁/n with four molecules in the unit cell and a calculated density of 1.667 g cm⁻³ at 123 K (Figure 1a).
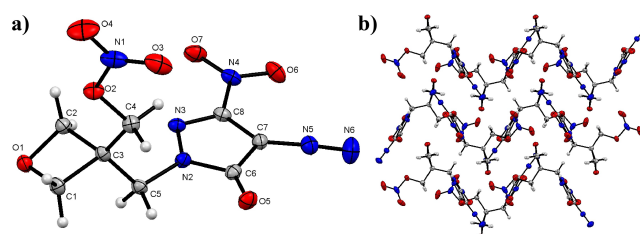

Figure 1. a) Molecular structure of **4** in the crystal. Thermal ellipsoids are drawn at the 50% probability level. **b)** View along the a axis – the molecules form a wave-like pattern.

The bond length of C6–O5 (1.218(2) Å) corresponds to a C=O double bond.[13] Further, C7–N5 has a length of 1.327(2) Å which is approximately the length of a C=N double bond.[14] The diazo group is nearly linear with an angle of 176.2° (C7–N5–N6) and shows a very short interatomic distance of 1.110(2) Å (N5–N6) which can be attributed to a N≡N triple bond. The angles within the oxetane ring range between 91.14(9)° at O1–C2–C3 and 91.52(9)° at O1–C1–C3. The smallest angle is observed at C1–C3–C2 (84.72(9)°). The oxetane ring shows a puckering angle of 12.5° which is slightly larger than the puckering angle found in unsubstituted oxetane (8.7°, 140 K).[15] The nitro group of the pyrazole motif essentially matches the pyrazole plane. In the crystal, the molecules are arranged to form a wave-like pattern along the a axis (Figure 1b).

Compound **7** crystallizes in the monoclinic space group P2₁/n with four formula units in the unit cell. The crystal

ChemPlusChem

Research Article
doi.org/10.1002/cplu.202200049

Chemistry Europe
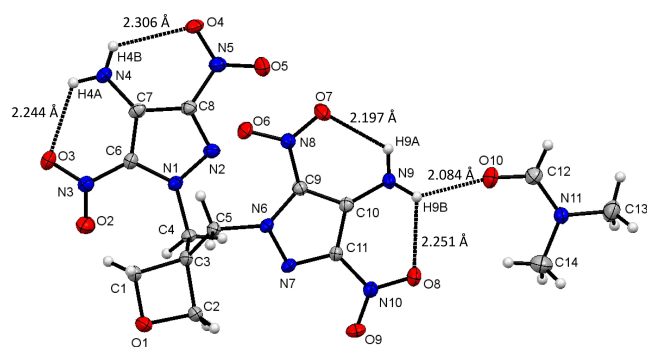European Chemical
Societies Publishing

Figure 2. Molecular structure of **7** in the crystal and interactions with the crystallized dimethylformamide molecule. Thermal ellipsoids are drawn at the 50% probability level.

contains one dimethylformamide molecule per formula unit and displays a density of 1.639 g cm^{-3} at 123 K (Figure 2).

The angles within the oxetane ring vary from 83.82(2)° at C1–C3–C2 to 91.72(2)° at O1–C2–C3. The oxetane ring is strongly folded with a puckering angle of 15.9° which is considerably larger than the corresponding angle in unsubstituted oxetane (8.7° at 140 K).[15] One of the pyrazole rings has both nitro groups in the ring plane, the other pyrazole ring has the nitro group at C6 twisted by 16.81° and the nitro group at C8 twisted by 3.28°. The amino group at C7 features intramolecular interactions with the neighbored nitro groups with distances of 2.306(2) Å and 2.244(2) Å. The other amino group at C10 shows the same interaction with distances of 2.197(2) Å and 2.251(2) Å. In addition, an intermolecular hydrogen bridge is found between this amino group and the oxygen atom of the dimethyl formamide molecule with a distance of 2.084(2) Å.

Compound **8** crystallizes in the monoclinic space group $P2_1/c$ with four formula units in the unit cell and a density of 1.608 g cm^{-3} at 123 K (Figure 3a). The angles within the oxetane motif vary from 84.72(2)° at C1–C3–C2 to 92.72(2)° at C1–O1–C3. The oxetane ring is found to be essentially planar and the azido group is almost linear (N1–N2–N3, 174.0(3)°). The nitro groups at C8 and C6 are twisted out of the pyrazole plane by 19.58° and 5.62°, respectively. The molecule displays an intramolecular hydrogen bond from H7B to O4 with a distance
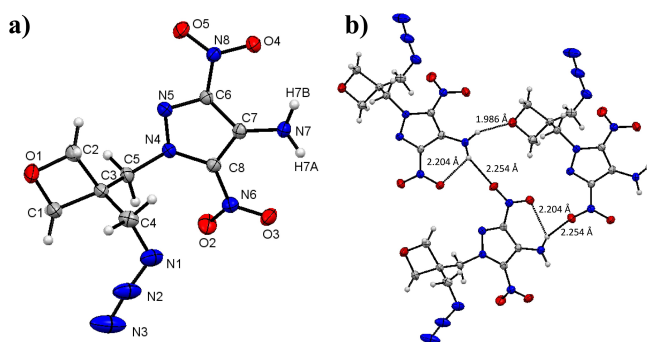
of 2.204(2) Å (Figure 3b). Further, there are intermolecular hydrogen bonds of the amino group to two adjacent molecules. One between H7B to O5 (nitro group) with a distance of 2.254(2) Å and another between H7A and O1 (oxetane ring) with a length of 1.986(2) Å. These hydrogen bonds contribute to a stabilization of the molecule in the solid state.

Compound **9A** crystallizes in the monoclinic space group $P2_1/c$ with four formula units in the unit cell and **9B** crystallizes in the triclinic space group $P-1$ with two formula units in the unit cell (Figure 4).
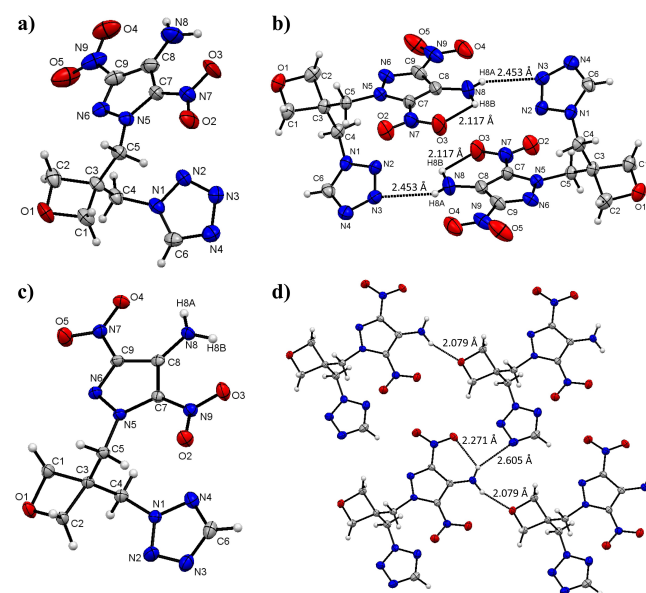

Figure 4. Molecular structure of **9A** (a) and the corresponding pairs formed in the solid state (b). Crystal structure of **9B** (c) and the network which is formed in the crystal (d). Thermal ellipsoids are drawn at the 50% probability level.

Compound **9B** has a density of 1.691 g cm^{-3} at 123 K which is marginally higher than the density of **9A** (1.630 g cm^{-3}) at 123 K. The puckering angle in the oxetane ring of **9B** is 14.5° while **9A** exhibits a way smaller puckering angle of 10.2°. For compound **9A**, two molecules arrange in pairs due to strong hydrogen bonding between the amino group and the tetrazole ring (N3) of a neighboring molecule with a distance of 2.453(5) Å. Intramolecular hydrogen bonding is found between the amino group (H8B) and an adjacent nitro group (O3) with a distance of 2.117(4) Å. An analogous intramolecular hydrogen bond is observed in case of compound **9B** involving H8A of the amino group and the neighboring oxygen atom O4 of the nitro group with a distance of 2.271(3) Å. In addition, H8A shows an intermolecular short contact bond to the tetrazole moiety (N3) of an adjacent molecule with a distance of 2.605(3) Å, which is quite long for a hydrogen bond. Moreover, an intermolecular short contact bond with a distance of 2.079(3) Å is found between H8B of the amino group and the oxetane oxygen atom O1 of a neighboring molecule.

Figure 3. a) Molecular structure of **8** in the crystal. Thermal ellipsoids are drawn at the 50% probability level. b) Intra- and intermolecular hydrogen bonding in the crystal structure of **8**.

Hirshfeld Analysis

When a mechanical force acts upon a solid energetic material, it causes vertical compression and horizontal sliding of layers in the crystal leading to internal strains.[16] If the related strain energy is higher than the lowest bond dissociation energy in the molecule, decomposition will occur.[17] In this context, intermolecular interactions can have a stabilizing or destabilizing effect establishing a direct correlation with an energetic materials' sensitivity.[17,18] A valuable tool to explore these interactions is Hirshfeld analysis.[19,20] Hence, we calculated the Hirshfeld surface (HFS) of all target compounds using CrystalExplorer V17.5 to find correlations.[21] On the HFS, close contact interactions are shown as red dots. In addition, we visualized all interactions and their distances $d_i + d_e$ (d_i = distance from HFS to the closest atom interior, d_e = distance from HFS to closest atom exterior) in a 2D fingerprint plot (Figure 5).[22]
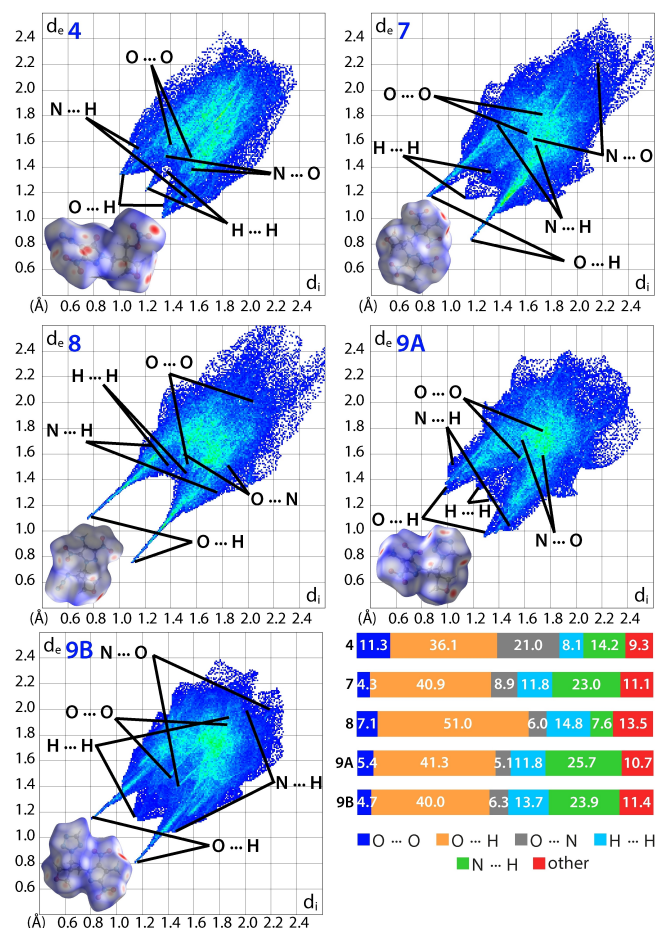

Figure 5. Calculated Hirshfeld surfaces and 2D fingerprint plots for compounds 4 and 7–9. The bar chart summarizes the respective populations of close contacts in the crystal.

Interactions with distances below 2.4 Å are considered strong while interactions with distances larger than roughly 3 Å are considered weak. Especially characteristic for sensitive compounds are high populations of repulsive O···O interactions next to destabilizing, repulsive O···N or H···H contacts. High sensitivity is particularly encountered when these are poorly balanced by stabilizing interactions like N···H or O···H close contacts.[17,18] Further, a comparison of the respective percentages (bar diagram, Figure 5) and the interaction distances ($d_i + d_e$) enables a weighting. This allows a reasonable estimation of the sensitivity and a ranking of the compounds relative to each other. For example, compound 4 shows stabilizing and strong ($d_i + d_e < 2.4$ Å) O···H interactions (36.1%) and moderately strong N···H (14.2%) interactions. These are counterbalanced by strong, repulsive H···H interactions and weak ($d_i + d_e > 3$ Å) destabilizing O···N (21.0%) and O···O interactions (11.3%). Even if these are weak, their high proportion significantly counteracts the stabilizing interactions. Therefore, a significant sensitivity toward mechanical stimuli can be anticipated. In comparison, compound 7 shows a significantly higher proportion of strong O···H interactions (40.9%). The stabilizing N···H interactions are weak, but their high proportion (23.0%) significantly contributes to the overall stabilization. With a total of 63.9%, they easily compensate found destabilizing interactions – these are made up by a low population of strong, repulsive H···H interactions (11.8%) next to weak O···N (8.9%) and O···O (4.2%) interactions with almost negligible proportions. As a consequence, low sensitivity can be expected. The highest population of strong O···H interactions (51.0%) is found in case of compound 8. Additional stabilization arises from of weak N···H interactions (7.6%). These are only attenuated by few and weak destabilizing interactions. Hereby, repulsive H···H interactions (14.8%) represent the largest fraction along with O···O and O···N interactions, with a cumulative share of only 13.1%. As stabilizing interactions (58.6%) clearly dominate, a low sensitivity is indicated. Since compounds 9A and 9B are regioisomers, very similar sensitivity might be expected. This is indeed reflected by very similar interaction proportions. Both compounds are equally dominated by strong O···H interactions with populations of 41.3% and 40%, respectively, and N···H interactions with high percentages of 25.7% and 23.9%. In compound 9A, this interaction has a higher significance, as the proportion is higher and the relative share of strong interactions ($d_i + d_e < 2.4$ Å) is more pronounced. The total population of stabilizing interactions is the highest of all investigated compounds with 67.0% (9A) and 63.9% (9B). Rather weak, repulsive H···H interactions impose a destabilizing effect on both 9A (11.8%) and 9B (13.7%). The same applies to O···N interactions with populations of 5.1% (9A) and 6.3% (9B) next to O···O interactions with proportions of 5.4% and 4.7%, respectively. Due to their low population and weak nature, they cause negligible destabilization. Based on found interactions, their population and respective strength, 9A and 9B should not only be very insensitive, but the least sensitive of all investigated compounds – closely followed by compounds 7 and 8 with compound 4 showing the highest sensitivity. This agrees well with the experimental values for impact and friction sensitivity (Table 2). However, an absolute difference in case of 7–9 cannot be quantified due their generally high insensitivity.
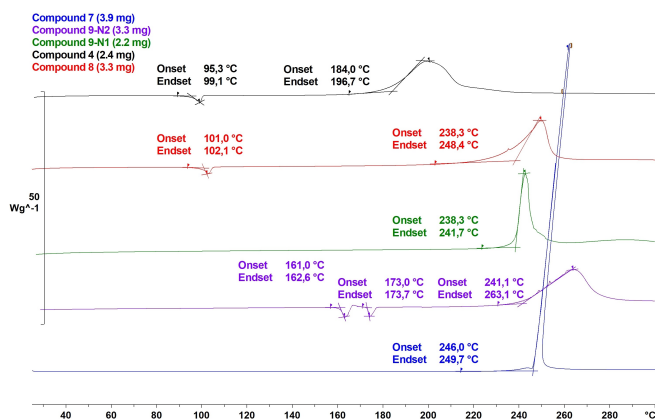
ChemPlusChem

Research Article
doi.org/10.1002/cplu.202200049

Chemistry Europe
European Chemical
Societies Publishing

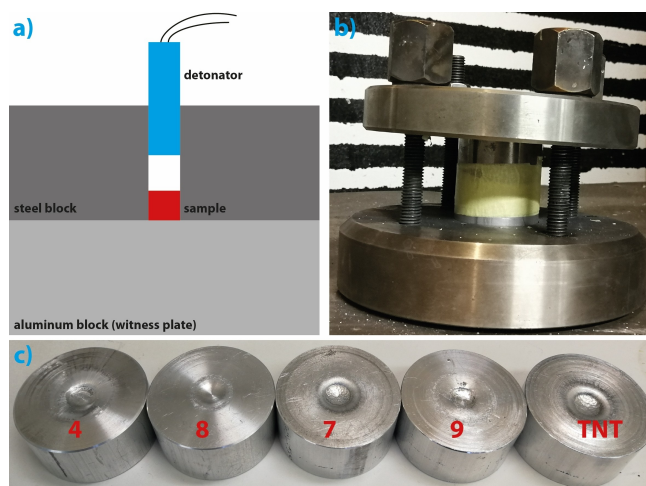**Figure 6.** DSC thermogram of compounds **4** and **7**–**9**.

Figure 7. a) Schematic setup of a SSRT. b) Steel block and witness plate confined between heavy steel plates prior to the test. c) Aluminum witness plates with dents caused by the respective sample.

Thermal analysis

Thermal analysis of all compounds was performed by differential scanning calorimetry (DSC) at a heating rate of $5\,°C\,min^{-1}$. Here, compound **4** shows the lowest melting point (95 °C) and due the presence of the diazonium and the nitrate ester moiety, which impose thermal instability, also the lowest decomposition temperature (184 °C) of all investigated compounds. Considerably higher decomposition temperatures were found for compounds **7**–**9**. Compound **8** shows a melting point at 101 °C and a decomposition temperature of 238 °C, which is very high as most organic azides already decompose at roughly 180 °C according to literature.[23] This can be attributed to stabilizing effects in the crystal (see Hirshfeld discussion). While isomer **9B** shows a phase transition at 161 °C, features a high melting point of 173 °C and decomposes at 241 °C, compounds **7** and **9A** do not show a melting point and directly decompose exothermically at 246 °C and 241 °C (Figure 6). The different and thus interesting thermal behavior of regioisomers **9A** (*N*1) and **9B** (*N*2) can be attributed to interactions in the crystal. In direct comparison, the *N*1-isomer shows a higher proportion of stabilizing interactions (O···H, N···H) and a lower proportion of repulsive H···H interactions (Figure 5). Specifically, the intermolecular hydrogen bond (H8 A–N3, d = 2.453 Å) is shorter and thus stronger than the analogous interaction in the *N*2 isomer with a distance of 2.605 Å. Further and contrary to the *N*2-isomer, parallel-displaced π-stacking interactions occur between spatially opposing pyrazole rings as well as tetrazole rings. In sum, the higher interactions prevent melting of **9A** prior to decomposition. Overall, **7** is the most thermostable compound of all, followed by **9B**, **9A**, **8** and organic nitrate **4**. As a result, the decomposition temperatures essentially correlate with the ratio of stabilizing and destabilizing effects in the crystal as indicated by Hirshfeld analysis. The effect of substitution is particularly interesting in case of compounds **7**–**9**, since the parent compound (ADNP) decomposes already at 183.6 °C when a heating rate of $10\,°C\,min^{-1}$ is applied.[24]

Small-scale shock reactivity and initiation test

In order to evaluate the explosive performance of compounds **4** and **7**–**9**, a small-scale shock reactivity test (SSRT) was performed (Figure 7).

This test is suitable to assess the shock reactivity (explosiveness) of an energetic material – often below its critical diameter and without requiring transition to detonation.[25] It combines the advantages of both lead block test and gap test while it requires small quantities of roughly 500 mg.[26] In each test, the same sample volume V_S is used (284 mm³) and the required amount of explosive (m_E) is calculated by the formula $m_E = V_S \cdot \rho_{XR} \cdot 0.95$ where ρ is the density determined via X-ray diffraction or helium pycnometry. Regarding the setup, each sample was pressed into a perforated steel block on top of an aluminum witness block with a pressure of three tons and five seconds duration. Subsequently, the arrangement is confined between two steel plates (Figure 7b). The pressed charge is then initiated by a commercial detonator (Orica Dynadet C2) using an air gap of 1.5 cm. The obtained dent sizes of the witness blocks can be compared to each other by filling them with finely powdered SiO_2 and measuring the respective weight. Alternatively, the actual dent volumes can be measured using a 3D profilometer. Hereby, the performance of the energetic materials can be compared relative to each other. As all investigated compounds show calculated performances comparable to 2,4,6-trinitrotoluene (TNT), it was used as reference. Interestingly, almost no indentation was obtained in case of compound **8** and plenty of unaffected material was found (see Supporting Information). In case of compounds **4**, **7** and **9**, significant dents were obtained, but much smaller than in case of TNT (Table 1) and thus far behind expectation. Since the critical diameter has little relevance in this test and its determination would require the detonation of numerous charges on a multigram scale at different charge diameters, the insensitivity of the investigated compounds was considered to

ChemPlusChem

Research Article
doi.org/10.1002/cplu.202200049

Chemistry
Europe
European Chemical
Societies Publishing

Table 1. Mass of explosive versus dent size in the SSRT.

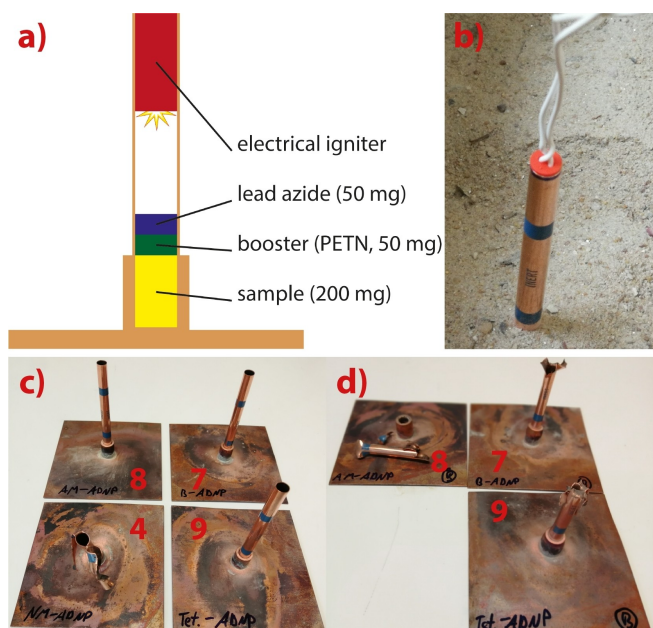| Compound	4	7	8	9	TNT
m_e (mg)	426	459	424	428	445
V_{dent} (mm^3)	160	298	34	162	343

Figure 8. a) Schematic test setup. b) Prepared charge in a sandbox. c) Negative (**7**, **8**, **9**) and positive result (**4**) using lead azide. d) Positive result using PETN as booster (**7**, **8**, **9**).

be the main cause. In this case, the applied shock impulse would be insufficient for a complete initiation rendering the results plausible. To prove this assumption, all compounds were subjected to a systematic initiation test in closed copper tubes with an inner diameter of 7 mm which is comparable to the SSRT diameter of 7.5 mm (Figure 8). Each tube was filled with 200 mg of the respective compound prior to pressing the charge (3 tons, 5 seconds). Afterward, each tube was charged with 50 mg of loosely packed military-grade lead azide (LA) and placed on top of a copper witness plate. Then, the primary explosive was initiated by the spark of an electrical ignitor. In case of compound **4**, the main charge (200 mg) was initiated by LA causing the destruction of the copper tube and an indentation of the witness plate. In case of compounds **7–9**, the copper tubes were left completely intact as only the LA top charge detonated proving the extreme insensitivity of these compounds (Figure 8c). Therefore, the test was repeated for compounds **7–9** using an additional booster charge of 50 mg pentaerythritol tetranitrate (PETN) which was pressed onto the sample charge and 50 mg of unpressed lead azide was again added prior to firing the charges with an electrical igniter. In all cases, the copper tube was destroyed and the witness plate perforated (**8**, **9**) or heavily dented (**7**) (Figure 8d). It can be concluded that all compounds except **4** are too insensitive to be initiated by the detonation of a lead azide primary charge. Instead, a booster explosive such as PETN is required for

initiation. Therefore, compounds **7–9** have proved to combine notable performance and thermostability with low sensitivity.

Energetic properties

All compounds were determined to be very insensitive toward impact and friction except **4** which is sensitive toward impact (3 J) but rather insensitive toward friction (288 N). All target compounds possess a combined nitrogen and oxygen content (N+O) between 63.4% (**9**) and 66.3% (**4**). The Gaussian16 program package was used to calculate the room temperature enthalpy of formation for all energetic target compounds at the CBS-4 M level of theory using the atomization method.[27,28] All compounds exhibit a positive heat of formation in a range of 105.2 to 263.0 kJ mol^{-1}. The EXPLO5 V6.04 code was used to calculate the energetic performance of compounds **4** and **7–9**. Isomers **9B** and **9A** show a calculated detonation velocity of 6820 ms^{-1} and 7088 ms^{-1} linked to detonation pressures of 16.7 and 18.3 GPa, respectively, which are therefore in the range of TNT (6809 ms^{-1}, 18.7 GPa). The same applies to azide **8** which features a comparable performance. In contrast, compounds **4** and **7** outperform TNT with detonation velocities of 7124 ms^{-1} and 7335 ms^{-1} and detonation pressures of 20.1 GPa and 20.9 GPa, respectively (Table 2). As compound **7** combines the highest performance and thermal stability of all presented compounds with great insensitivity, it is probably the most promising compound for the preparation of future energetic binders with superior characteristics in these aspects. With respect to performance, all compounds are superior to state-of-the-art energetic oxetane monomers (Table S5 (Supporting Information) and Table 2). With exception of compound **4**, this also applies to the thermal stability.

Conclusion

The synthesis of BMHMO (**1**) was significantly improved compared to literature methods to provide a yield of 85% (+33%) rendering it an inexpensive and versatile precursor for the synthesis of both energetic and non-energetic oxetanes. Substitution using K-ADNP (**2**) afforded alcohol **3** in quantitative yield which can directly provide various energetic monomers using suitable electrophiles (**4**). Beyond, mesylation gave sulfonic ester **5** which was used to obtain symmetric compound **7** and asymmetric derivatives **8** and **9** in high yield. With exception of compound **4**, all compounds show an interplay of performance, thermostability, and insensitivity unparalleled in the field of energetic oxetanes and exhibit an advantageous, positive heat of formation. Their calculated performance is in range of the standard military explosive TNT (**8**, **9**) or even higher (**4**, **7**). Thus, they are clearly superior to typical energetic oxetane monomers which constitute the current state of the art (e.g., NIMMO, AMMO, BAMO). The molecular structures of all compounds were elucidated by single crystal X-ray diffraction allowing a sensitivity estimation via Hirshfeld analysis next to the practical evaluation. Compound **4** was found to be rather

ChemPlusChem

Research Article
doi.org/10.1002/cplu.202200049

**Chemistry
Europe**
European Chemical
Societies Publishing

Table 2. Physiochemical properties of compounds **4, 7, 8, 9A** and **9B** in comparison to **NIMMO** and **TNT**.

	4	**7**	**8**	**9A (N1)**	**9B (N2)**	**NIMMO**	**TNT**
Formula	$C_8H_8N_6O_7$	$C_{11}H_{12}N_{10}O_9$	$C_8H_{10}N_8O_5$	$C_9H_{11}N_9O_5$	$C_9H_{11}N_9O_5$	$C_5H_9NO_4$	$C_7H_5N_3O_6$
FW [g·mol^{-1}]	300.19	428.28	298.22	325.27	325.27	147.13	227.12
IS[a] [J]	3	>40	>40	>40	>40	>40	15
FS[b] [N]	288	>360	>360	>360	>360	360	>353
N/N+O[c] [%]	28.0/65.3	32.7/66.3	37.6/64.4	38.8/63.4	38.8/63.4	9.5/52.2	18.5/60.5
Ω_{CO}, Ω_{CO2}[d] [%]	−26.6, −69.3	−29.9, −71.0	−42.9, −85.8	−46.7, −91.0	−46.7, −91.0	−59.8, −114	−24.7, −74.0
T_m[e]/$T_{dec.}$[f] [°C]	95/184	–/246	101/238	–/238	161/241	−14/170	81/290
ρ[g] [g·cm^{-3}]	1.62	1.70	1.56	1.64	1.59	1.19	1.64
ΔH_f°[h] [kJ·mol^{-1}]	115.2	105.2	315.3	238.0	263.0	−268.9	−219.0
EXPLO5 V6.04							
$-\Delta E_U^{\circ}$[i] [kJ·kg^{-1}]	4634	4206	4244	3769	3682	3949	4380
T_{C-J}[j] [K]	3276	2981	2948	2669	2649	2507	3190
D_{C-J}[k] [m·s^{-1}]	7124	7335	6962	7088	6820	5906	6809
p_{C-J}[l] [GPa]	20.1	20.9	17.8	18.3	16.7	10.6	18.7
V_0[m] [dm^3·kg^{-1}]	707	710	746	730	734	827	640

[a] Impact sensitivity (BAM drop hammer, method 1 of 6). [b] Friction sensitivity (BAM friction apparatus, method 1 of 6). [c] Nitrogen and oxygen content. [d] Oxygen balance with regard to carbon monoxide ($\Omega CO=(nO-xC-yH/2)(1600/FW)$) and carbon dioxide ($\Omega CO_2=(nO-2xC-yH/2)(1600/FW)$). [e] Melting point (DSC, $\beta=5\,°C\cdot min^{-1}$). [f] Temperature of decomposition (DSC, $\beta=5\,°C\cdot min^{-1}$). [g] Density at 298 K (ρX-ray/1.028) or helium pycnometry (**7**). [h] Standard molar enthalpy of formation. [i] Detonation energy. [j] Detonation temperature. [k] Detonation velocity. [l] Detonation pressure. [m] Volume of detonation products (assuming only gaseous products).

sensitive, while compounds **7–9** are highly insensitive which was also reflected by the SSRT and initiation test. Like other energetic oxetanes we are studying, **4** and **8** show melting points around 100 °C. Hence, higher performances may even allow oxetanes to enter the field of melt-cast explosives. For now, compounds **7–9** are most well-suited to prepare low-sensitivity energetic binders with enhanced performance to be applied in low-vulnerability ammunitions (LOVA). Unfortunately, the steric demand of compound **7** is very likely to complicate its homopolymerization. However, copolymerization with sterically less demanding compounds (e.g., THF) may even benefit from the bulky substituents as back-biting reactions become effectively suppressed. Based on the current results, we conclude that BMHMO and ADNP are promising structural motifs for the synthesis of energetic monomers surpassing the prior art in key-aspects like performance, sensitivity and thermostability. We anticipate that these motifs and the investigated compounds are helpful to develop the next generation of energetic binders and to lessen the lack of available monomers for their preparation.

Experimental Section

A Supporting Information is available comprising the following: Synthetic procedures, ^{1}H, ^{13}C, ^{14}N NMR spectra, Crystallographic information, DSC graphs, Hot-plate test of compounds **4, 7–9** (video, hot-plate test.mp4).

Deposition Numbers 2097524 (for **3**), 2097531 (for **4**), 2097526 (for **5**), 2097528 (for **6**), 2097525 (for **7**), 2097527 (for **8**), 2097530 (for **9A**), 2097529 (for **9B**) contain the supplementary crystallographic data for this paper. These data are provided free of charge by the joint Cambridge Crystallographic Data Centre and Fachinformationszentrum Karlsruhe Access Structures service.

Conflict of Interest

The authors declare no conflict of interest.

Data Availability Statement

The data that support the findings of this study are available from the corresponding author upon reasonable request.

[1] H. G. Ang, S. Pisharath, in *Energetic Polymers: Binders and Plasticizers for Enhancing Performance*, Wiley-VCH, Germany, **2012**.
[2] T. M. Klapötke, in *Chemistry of High-Energy Materials*, 5th ed., deGruyter, Berlin/Boston, **2019**.
[3] M. S. Kirshenbaum, L. Avrami, B. Strauss, in *Sensitivity Characterization of low vulnerability (LOVA) propellants*, US Army Armament Research and Development Command, **1983**.

ChemPlusChem

Research Article
doi.org/10.1002/cplu.202200049

Chemistry Europe
European Chemical
Societies Publishing

[4] G. E. Manser, A. A. Malik, T. G. Archibald, in *3-Azidomethyl-3-Nitromethyloxetane*, US 5489700, **1996**.

[5] M. P. Dreyfuss, P. Dreyfuss, *Oxetane Polymers. In Encyclopedia of Polymer Science and Technology*, Wiley, Hoboken, New Jersey, **2011**.

[6] V. M. Vinogradov, T. I. Cherkasova, I. L. Dalinger, S. A. Shevelev, *Russ. Chem. Bull.* **1993**, *42*, 1552.

[7] S. Ek, N. V. Latypov, *J. Heterocycl. Chem.* **2014**, *51*, 1621.

[8] T. M. Klapötke, in *Energetic Materials Encyclopedia*, DeGruyter: Berlin/Boston, **2021**.

[9] Y. Zhang, Y. Huang, D. A. Parrish, J. M. Shreeve, *J. Mater. Chem.* **2011**, *21*, 6891.

[10] D. Fischer, J. L. Gottfried, T. M. Klapötke, K. Karaghiosoff, J. Stierstorfer, T. G. Witkowski, *Angew. Chem. Int. Ed.* **2016**, *55*, 16132.

[11] M.-X. Zhang, P. F. Pagoria, G. H. Imler, D. J. Parrish, *Heterocycl. Chem.* **2019**, *56*, 781.

[12] L. Dalinger, I. T. Cherkasova, A. Shevelev, *Mendeleev Commun.* **1997**, *7 (2)*, 58–59.

[13] A. G. Orpen, L. Brammer, F. H. Allen, O. Kennard, D. G. Watson, R. Taylor, in *Struct. Correl.* **1994**, p. 752.

[14] P. F. de Athayde-Filho, J. Miller, A. M. Simas, B. F. Lira, J. A. de Souza Luis, J. Zuckerman-Schpector, *Synthesis* **2003**, *5*, 685.

[15] P. Luger, J. Buschmann, *J. Am. Chem. Soc.* **1984**, *106*, 7118.

[16] J. Zhang, Q. Zhang, T. T. Vo, D. A. Parrish, J. M. Shreeve, *J. Am. Chem. Soc.* **2015**, *137*, 1697.

[17] M. Reichel, D. E. Dosch, T. M. Klapötke, K. Karaghiosoff, *J. Am. Chem. Soc.* **2019**, *141*, 19911.

[18] M. Reichel, M. Born, D. E. Dosch, T. M. Klapötke, K. Karaghiosoff *Cryst. Growth Des.* **2021**, *21*, 243.

[19] M. A. Spackman, D. Jayatilaka, *CrystEngComm* **2009**, *11*, 19.

[20] J. J. McKinnon, M. A. Spackman, A. S. Mitchell, *Acta Crystallogr. Sect. B* **2004**, *60*, 627.

[21] M. J. Turner, J. J. McKinnon, S. K. Wolff, D. J. Grimwood, P. R. Spackman, D. Jayatilaka, M. A. Spackman, in *CrystalExplorer17* (**2017**). University of Western Australia. https://hirshfeldsurface.net.

[22] M. A. Spackman, J. J. McKinnon, *CrystEngComm* **2002**, *4*, 378.

[23] T. Keicher, S. Löbbecke, in *Organic Azides*; John Wiley & Sons: Hoboken, New Jersey, **2010**.

[24] R. D. Schmidt, G. S. Lee, P. F. Pagoria, A. R. Mitchell, R. Gilardi, *J. Heterocycl. Chem.* **2001**, *38*, 1227.

[25] J. E. Felts, H. W. Sandusky, R. H. Granholm, in *AIP Conference Proceedings 2009*, American Institute of Physics, Vol. 1195, pp 233–236.

[26] R. Meyer, J. Köhler, A. Homburg, in *Explosives*, 6th ed.; Wiley-VCH: Weinheim, **2007**.

[27] M. J. Frisch, G. W. Trucks, H. B. Schlegel, G. E. Scuseria, M. A. Robb, J. R. Cheeseman, G. Scalmani, V. Barone, G. A. Petersson, H. Nakatsuji, X. Li, M. Caricato, A. V. Marenich, J. Bloino, B. G. Janesko, R. Gomperts, B. Mennucci, H. P. Hratchian, J. V. Ortiz, A. F. Izmaylov, J. L. Sonnenberg, D. Williams-Young, F. Ding, F. Lipparini, F. Egidi, J. Goings, B. Peng, A. Petrone, T. Henderson, D. Ranasinghe, V. G. Zakrzewski, J. Gao, N. Rega, G. Zheng, W. Liang, M. Hada, M. Ehara, K. Toyota, R. Fukuda, J. Hasegawa, M. Ishida, T. Nakajima, Y. Honda, O. Kitao, H. Nakai, T. Vreven, K. Throssell, J. A. Montgomery, Jr., J. E. Peralta, F. Ogliaro, M. J. Bearpark, J. J. Heyd, E. N. Brothers, K. N. Kudin, V. N. Staroverov, T. A. Keith, R. Kobayashi, J. Normand, K. Raghavachari, A. P. Rendell, J. C. Burant, S. S. Iyengar, J. Tomasi, M. Cossi, J. M. Millam, M. Klene, C. Adamo, R. Cammi, J. W. Ochterski, R. L. Martin, K. Morokuma, O. Farkas, J. B. Foresman, D. J. Fox, Gaussian16, Gaussian, Inc., Wallingford, CT, USA, **2016**.

[28] T. Altenburg, T. M. Klapötke, A. Penger, J. Stierstorfer, *Z. Anorg. Allg. Chem.* **2010**, *636*, 463.